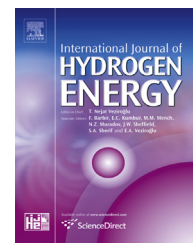




ELSEVIER

Available online at [www.sciencedirect.com](http://www.sciencedirect.com)

ScienceDirect

journal homepage: [www.elsevier.com/locate/he](http://www.elsevier.com/locate/he)

# Dynamic programming technique for optimizing fuel cell hybrid vehicles

Dima Fares <sup>a,\*</sup>, Riad Chedid <sup>a</sup>, Ferdinand Panik <sup>b</sup>, Sami Karaki <sup>a</sup>,  
Rabih Jabr <sup>a</sup>

<sup>a</sup> Electrical and Computer Engineering Department, American University of Beirut, Beirut, Lebanon

<sup>b</sup> Mechanical Engineering Department, University of Applied Science, Esslingen, Germany

## ARTICLE INFO

### Article history:

Received 1 September 2014

Received in revised form

11 December 2014

Accepted 28 December 2014

Available online 17 January 2015

### Keywords:

Fuel cell hybrid vehicle (FCHV)

Hybrid power system

Energy management system (EMS)

Improved dynamic programming

(IDP)

## ABSTRACT

Transportation industries are incorporating fuel cell hybrid vehicles to lower the levels of polluting emissions. This paper develops a dynamically efficient energy management system for the purpose of achieving an optimal power allocation between the energy sources while adhering to component requirements and maintaining the required operational performance using a weighted improved dynamic programming technique. A power train configuration with a fuel cell dominant model based on a Simulink architecture of the electric vehicle is used for testing the energy management system. Two stage control methodologies are addressed, pre-driving off-line optimization using weighted improved dynamic programming algorithm and on-line optimization using PID controller. The technique proves convergence faster than normal dynamic programming algorithms which suffer from dimensionality problems. Weights are incorporated in the fitness function in-order to improve convergence rate of such a method with long duration driving cycles. The performance criteria is based on the overall operational cost as well as the hydrogen consumption per trip. The stress on the vehicle sources is approximated based on a haar wavelet transform of the instantaneous power. Results indicate lower costs and hydrogen consumption levels using the weighted improved dynamic programming as compared to the rule based algorithms.

Copyright © 2015, Hydrogen Energy Publications, LLC. Published by Elsevier Ltd. All rights reserved.

## Introduction

There is an increasing awareness regarding the danger of polluting emissions and the drainage of energy resources. The transportation sector is one of the main sectors contributing to the emissions of such pollutants. Therefore, trends are adopted in-order to develop new policies and trigger

technological improvements in an attempt to surmount these effects. Fuel cell hybrid vehicles (FCHV) is one promising candidate. FCHV with battery storage systems have low emissions, high energy efficiency and independence on fossil fuel based resources.

There is a wealth of papers that address the design of the energy management systems in FCHV [1–3]. A comprehensive review of the state of art of FCHV architectures along with the

\* Corresponding author. Department of Electrical and Computer Engineering, American University of Beirut, P.O. Box 11-0236, Riad El Solh, Beirut 1107 2020, Lebanon. Tel.: +961 3 809859.

E-mail address: [daf03@aub.edu.lb](mailto:daf03@aub.edu.lb) (D. Fares).

<http://dx.doi.org/10.1016/j.ijhydene.2014.12.120>

0360-3199/Copyright © 2015, Hydrogen Energy Publications, LLC. Published by Elsevier Ltd. All rights reserved.

most tackled approaches in EMS is presented by Bayindir and Erdinic et al. [4,5]. A comparative analysis between the different methods for the optimal power allocation is discussed by Motapon et al [6]. Dynamic programming (DP) is a popular technique of choice for the optimal power allocation of FCHV. It is widely used and adopted to control the degree of hybridization between the vehicle sources whether internal combustion engine (ICE) based [7] or purely electrical. It is used for solving recursive problems and it ensures optimality within certain tolerance and depicts ease of implementation [8]. The main problem with DP is the curse of dimensionality where the number of states increases exponentially with time [9].

In Ref. [10], the HEV power sources are the ICE and the battery system. DP is used to test the effect of battery weight and storage capacity on the operational cost. The analysis leads to the selection of the most feasible battery capacity to lower system costs. Vinot et al. [11] used DP for an electric vehicle with ICE. The program locates the optimal split factor between the engine and the motor, as well as locating the optimum operating point of the engine. Xu et al. [12], developed a controller based on dynamic programming where the cost of FC and battery are minimized while subjected to limit constraints. The authors introduced a penalty factor on the battery state of charge (SOC) where the cost increases cubically if SOC is outside the limit margin. Dokuyucu et al. [13] formulated a controller based on dynamic programming to find the torque split between the ICE and the electric motor. The control signal considered is the battery SOC which is bounded between 0.4 and 0.7. Results show that during low torque demands, the vehicle operates in motor mode and charging is favored. While during high torque demands, both the battery and the ICE assist in feeding the load. They analyzed two different series parallel architectures for the HEV, using an electric variable transmission concept which leads to slightly higher fuel consumption range, but it can be tweaked by using a gear between the engine and motor.

To address the dimensionality constraint limitation of DP, improved dynamic programming technique (IDP) is used. To guarantee faster convergence weights are added to the fitness function. This novel method considers a tunnel of fixed states rather than an exponential increase in the number of states. In Ref. [14], power levels of fuel cell are considered in the state vector while in Ref. [15] the authors take SOC levels as state vectors. Both latter papers consider the improved DP and the results are not far from using the regular DP.

This paper tackles contemporary issues in the energy management system of the FCHV. Two stage control methodologies are defined, pre-driving optimization algorithms and on-line optimization using PID controller. In the first stage, a weighted improved dynamic programming technique is used to find the sub-optimum power allocation for the whole cycle. The weighting factor also substitutes the commonly used cost function which adds speed to the program. MatLab pre-allocation feature is incorporated to further reduce the computation time of such an algorithm. This is an off-line model of the EMS to help find the optimal power allocation. On-line optimization is performed using a complete Simulink designed model of the fuel cell hybrid vehicle. During the on-line operation the optimal power allocation

data derived from the off-line mode is injected into the EMS of the Simulink model. The weighted improved dynamic programming is used to test the efficiency of such algorithm in lowering operational cost while ensuring drivability. A PID controller minimizes the error between the actual and approximated vehicle speeds.

## Modeling the FCHV power train

The construction of the FCHV subsystem models in a graphical simulation environment software is widely exploited in literature. It is essential for the models to emulate the real dynamics of the vehicle in-order to have efficient simulation results [16–19]. In this paper, the vehicle considered is a light duty sprinter shown in Fig. 1, composed of at least seven different subsystems as indicated in Table 1.

The sources in the subsystem are a primary one-way energy source unit and a secondary bi-directional storage component. The former source is a PEM fuel cell system and the latter is a Lithium ion battery. The battery system is connected to the DC bus via a bi-directional DC/DC converter. The FC is directly coupled to the DC bus. The DC bus supplies the vehicle auxiliaries with DC power which will be transformed to AC by inverter. The auxiliary path is split in two branches one with DC/DC to the lower 24 V DC board net and the other with DC/AC to the electric drives for the sub-components such as water pumps and air conditioning. The power train of the vehicle is supplied by an AC motor which is connected to the DC bus via a DC/AC inverter.

The mathematical models that govern these subsystems encompass high levels of computational complexity. For this reason, simple dynamic equations as well as test-benched experimental results indexed as lookup tables are used to model the subsystems in the Simulink model. An energy management system strategy based on optimization algorithms is formulated to coordinate the power split between the sources.

## Fuel cell system modeling

Fuel cell systems are composed of cells that convert the chemical energy present in hydrogen fuel into electrical energy by oxidation–reduction reaction. Their transient

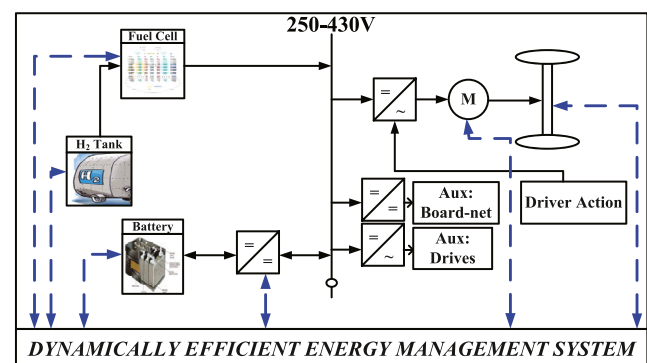


Fig. 1 – FCHV topology.

**Table 1 – FCHV subsystems.**

Subsystem	Description
FC system	70 kW PEM FC
Battery system	6.5 Ah Li-ion
DC/DC converter	Bi-directional
Electric motor	70 kW induction AC motor
Vehicle dynamics	Dynamic models of forces
Drivers model	Torque demand calculation
EMS	Optimal power allocation

performance when responding to load demand is limited due to the chemical reactions that occur in the FC. FC high cost can be cut via volume production of units for automotive applications. Improvements of the FC system is achieved along with enhancing the supervisory control between the FC and its converters to monitor the flow of reactants and maintain the voltage on the DC bus [20].

In this section, a static model of a PEM FC is selected consisting of 350 cells ( $n_{st}$ ) in series. To avoid complex chemical equations of the FC, the net power output ( $P_{FC}$ ) of the fuel cell is shown in equation (1), where the power demanded by the compressor ( $P_{comp}$ ), the FC auxiliaries ( $P_{FC-aux}$ ) and system losses ( $P_{FC-losses}$ ) is deducted from the power supplied by the stack. The latter is a function of the number of cells, the stack voltage ( $V_{st}$ ) and the stack current ( $I_{st}$ ). The auxiliary components in the FC are the radiator fan, coolant pump and others.

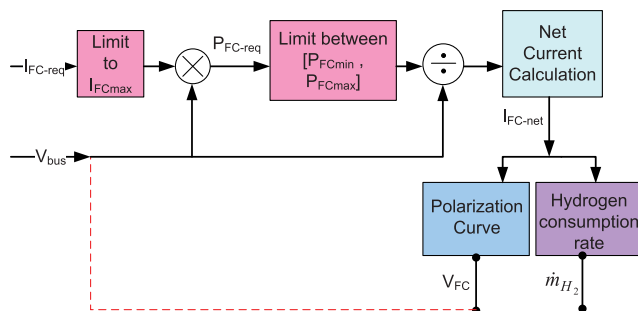
$$P_{FC} = n_{st}V_{st}I_{st} - P_{comp} - P_{FC-aux} - P_{FC-losses} \quad (1)$$

To consider the life cycle cost of the FC system, the current production cost is approximated to \$50/kW with a volume manufacturing of 500,000 units per year [21]. The service life of automotive fuel cells is around 5000 h. Therefore, a service life cost measure ( $\gamma_{SL-FC}$ ) of an FC is indicated in equation (2).

$$\gamma_{SL-FC} = 0.01 \text{ \$/kWh} \quad (2)$$

To build a fast and correct Simulink model of the FC, lookup tables based on experimental testing of an actual FC test-bench are used. Fig. 2, shows a schematic of FC system incorporated in the Simulink model.

The current requested from the FC ( $I_{FC-req}$ ) is limited to the maximum current ( $I_{FCmax}$ ) that could be supplied by the FC according to the manufacturers data sheet. Then, the power required from the FC is calculated by multiplying the requested current with the corresponding voltage of the DC bus ( $V_{bus}$ ). The FC power request ( $P_{FC-req}$ ) is also limited

**Fig. 2 – Fuel cell Simulink block diagram.**

between the maximum ( $P_{FCmax}$ ) and minimum ( $P_{FCmin}$ ) power of the FC that is provided in the data sheet. From the resulting FC current request, the net current request is computed using the net current curve in Fig. 3a. Then, the net current is used to calculate the FC voltage using the polarization curve in Fig. 3b. This takes into consideration the losses in the FC system such as activation and ohmic losses as well as accounting for the power needed to drive the compressor. The stack voltage is a function of the stack current and the cathode pressure. This voltage is the same voltage as the DC bus voltage because the FC system is directly connected to the DC bus. Finally, using the net FC current request, the hydrogen consumption is approximated using the hydrogen consumption curve in Fig. 3c and d.

The nonlinear relation between the power provided by the FC and the respective hydrogen consumed is modeled. The data is used in the Simulink model and derived from experimental testing on the FC system. Equation (3) provides the curve fitting model to be used during off-line simulations.

$$\dot{m}_{H_2}(P_{FC}) = 3.9 \times 10^{-5}P_{FC}^2 + 0.012P_{FC} - 0.0031 \quad (3)$$

At an energy cost of 8 cents/kWh, the price of hydrogen production ranges from 14 to 16 \$/kg [22]. An average cost for hydrogen of 15 \$/kg is used. The value for the cost of energy from hydrogen consumption can be approximated from the consumption of hydrogen per kWh. The latter variable is the slope of Fig. 3d which is approximated to be 0.015 g/kWh. The hydrogen cost ( $\gamma_{FC}$ ) is approximated in equation (4).

$$\gamma_{FC} = 0.015 \times 3600 \times 0.015 = 0.81 \text{ \$/kWh} \quad (4)$$

In this paper, the characteristics of the chosen FC is shown in Table 2.

### Battery system

The next building block of the FCHV power-train is the battery system. The model used for the battery is the internal resistance model where the open circuit voltage ( $V_{BT-oc}$ ), the internal resistance ( $R_{BT}$ ) and the battery power ( $P_{BT}$ ) are functions of the SOC. The mathematical relations governing this dependency is shown in equations (5) and (6). The SOC is derived by integrating the battery current ( $I_{BT}$ ) at time step  $k$  ( $t_k$ ). The value is divided by the battery capacity ( $C_{BT}$ ).

$$I_{BT} = \frac{V_{BT-oc} - \left( \sqrt{V_{BT-oc}^2 - 4R_{BT}P_{BT}} \right)}{2R_{BT}} \quad (5)$$

$$SOC(t_k) = SOC(0) - \frac{1}{C_{BT}} \int_{t_0}^{t_k} I_{BT} dt \quad (6)$$

The Simulink model for the battery is shown in Fig. 4. It receives the battery current request and accordingly computes the battery voltage depending on the SOC, internal resistance and temperature ( $T_{amb}$ ). It is composed of four different blocks that are interconnected. These blocks are the SOC generator block, the open circuit voltage generator block, the battery resistance generator block and the thermodynamics block.

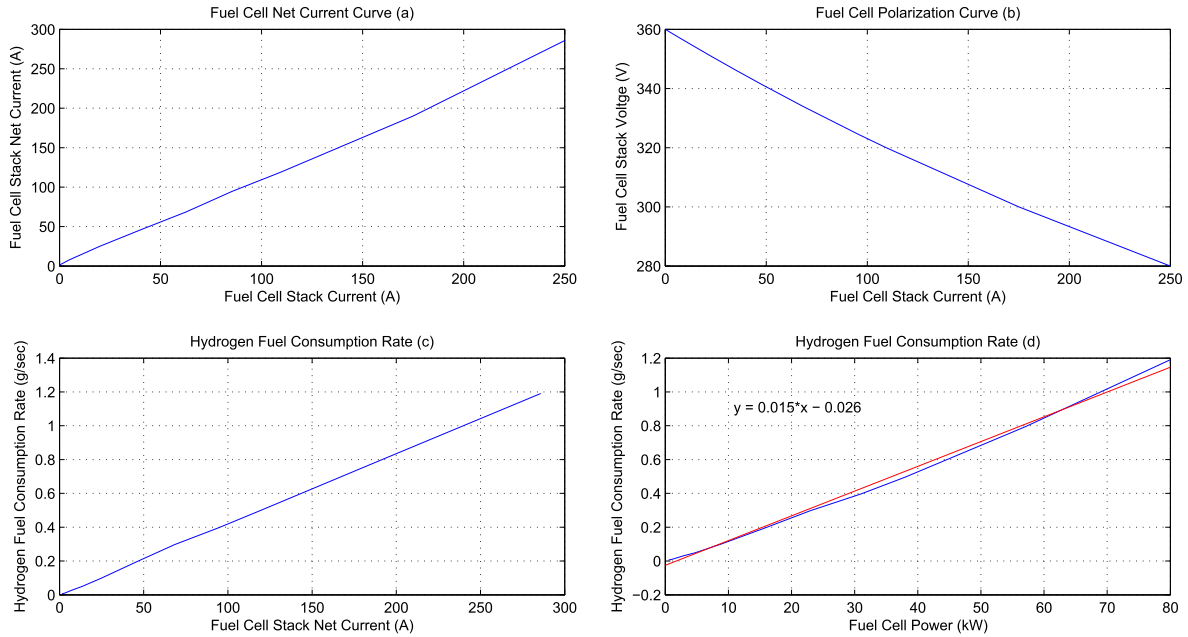


Fig. 3 – Fuel cell characteristic curves.

In the SOC generation block, the SOC is updated from the current value inputted to the block as shown in equation (6). The open circuit voltage generation block adds the effects of SOC and temperature on the battery open circuit voltage according to equation (7).

$$V_{BT-oc} = \beta_{BT} V_{BT-oc0} + (\alpha_{OCV}(T_{BT} - T_{amb}))(n_{BT}) \quad (7)$$

The open circuit voltage depends on the current SOC level so  $V_{BT-oc0}$  is estimated according to Fig. 5a by a factor  $\beta_{BT}$ . Then the battery voltage can be derived accordingly depending on the ambient temperature and the actual battery temperature ( $T_{BT}$ ). The temperature difference is multiplied by the number of battery cells ( $n_{BT}$ ) and a temperature coefficient ( $\alpha_{OCV}$ ). Note that at the beginning of the simulation the battery temperature is equal to the ambient temperature.

The battery internal resistance for a certain level of SOC and for a specific battery temperature is calculated using the method in equation (9). Fig. 5b and c, indicate the resistive factor ( $\alpha_{R-SOC}$ ) added to the battery during charging and discharging processes depending on the SOC level as shown also in equation (8). Similarly, Fig. 5d shows the relation between resistance and battery temperature ( $\alpha_{R-T}$ ) as shown also in equation (8).

$$\alpha_{R-SOC} = f(SOC) \quad \alpha_{R-T} = f(T_{BT}) \quad (8)$$

Therefore, after interpolating the factors  $\alpha_{R-SOC}$  and  $\alpha_{R-T}$  using Fig. 5b–d respectively, the battery internal resistance can be computed using equation (9).

$$R_{BT} = \alpha_{R-SOC} \alpha_{R-T} \quad (9)$$

To calculate the temperature changes in the battery in degrees Celsius, a simple equation is adopted based on the thermodynamic system inside the battery. It is the continuous integration of three factors divided by the heat capacity of the battery ( $H_{BT}$ ) as shown in equation (10).

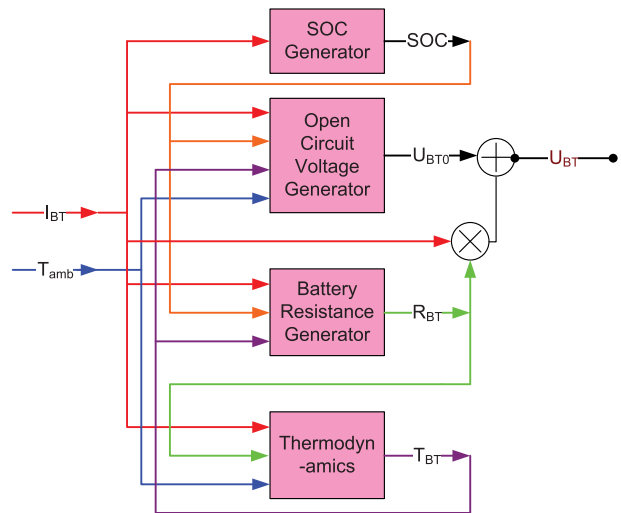


Fig. 4 – Battery Simulink model.

Table 2 – Fuel cell characteristic table.

FC variable	Value
Ramp up/down rates [kW/s]	[10, -10]
Max/min power [kW]	70/0
Number of cells	350
Minimum voltage [V]	280
Maximum voltage [V]	360

$$T_{BT} = \frac{1}{H_{BT}} \int [(I_{BT}^2 R_{BT}) + [n_{BT} I_{BT} \delta_{siBT} (T_{BT} + 273)] + 32(T_{amb} - T_{BT})] \quad (10)$$

The first factor is the heat loss by the current, the second is the entropy generator which multiplies the battery current, the number of cells and temperature in Kelvin by an entropy of cell reaction factor ( $\delta_{siBT}$ ). Finally, the third factor is the difference between the ambient and battery temperature multiplied by the battery thermal resistance which depends on the power in each cell with respect to the area. Finally, the output voltage of the battery system ( $V_{BT}$ ) is calculated using equation (11).

$$V_{BT} = V_{BT-oc} + R_{BT} I_{BT} \quad (11)$$

The average number of cycles for the battery used in vehicular applications is 1000 [23]. With an approximate battery price per kW of \$600 [24], the battery life-cycle cost ( $\gamma_{BT}$ ) is approximated as shown in equation (12).

$$\gamma_{BT} = 0.6 \text{ \$/kWh} \quad (12)$$

During off-line simulations, the losses of energy sources are also taken into consideration using Q-maps. Q maps are used to model the losses in the battery, which include the power value of the battery while considering internal resistance losses, charge losses and other battery losses. These Q-maps are derived from test-benches where actual battery values are measured [25]. Fig. 6, shows a Q-map for a battery derived in Ref. [25]. To approximate the losses, the basic fitting equation given in equation (13) is used.

$$Q_{BT}(P_{BT}) = -0.0076P_{BT}^2 - 1.1P_{BT} + 0.4 \quad (13)$$

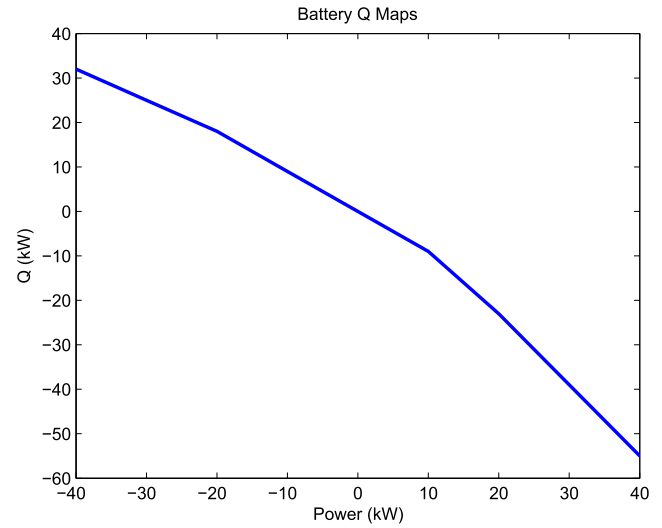


Fig. 6 – Battery Q maps.

### Drivers model subsystems

The driving cycle is usually indexed by a velocity profile. The drivers model subsystem is responsible to send control signals to the energy management system. These signals represent the magnitude of the accelerating and braking torques. The derivation of these signals is based on the reference speed set by the user and the actual vehicle speed measured at the level of the wheels. In order to minimize the speed difference between the referenced value and the measured value, a proportional integral derivative controller (PID) is adopted. This

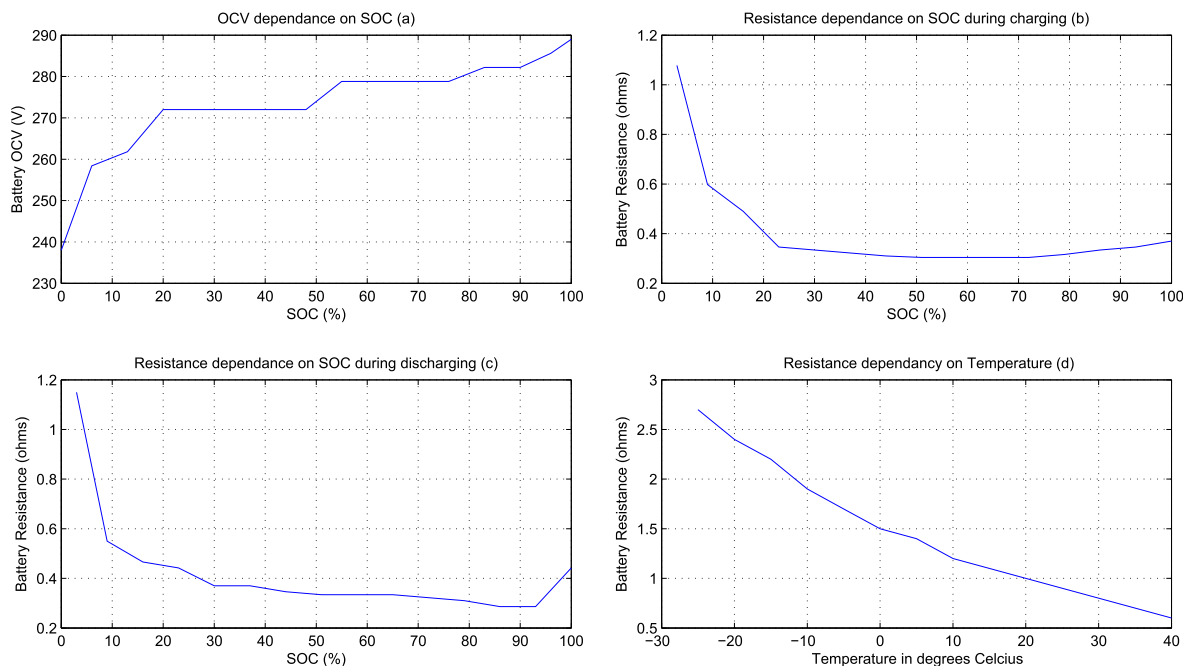


Fig. 5 – Battery characteristic curves.

**Table 3 – Vehicle model characteristic table.**

Vehicle variable	Value
Total mass $m$ (kg)	3500
Frontal area $A_f$ (m <sup>2</sup> )	3.48
Drag coefficient $C_d$	0.44
Traction coefficient $\mu_r$	0.9
Air density $\rho_{air}$ (kg/m <sup>3</sup> )	1.29
Tyre radius $R_w$ (m)	0.314
Wheels moment of inertia $\theta_w$ (kg m <sup>2</sup> )	3.2
Maximum braking force $f_{br-max}$ (m/s <sup>2</sup> )	0.8
Center of gravity $Cog$ (m)	0.314
Wheel base $w_b$ (m)	2.778
Axle load distribution $\mu_{al}$	0.5

type of controllers is widely used in the control systems in order to minimize the error between the measured and the desired process value.

### Vehicle dynamics subsystem

The forward model for vehicle dynamics is adopted. The parameters of the light duty sprinter are shown in Table 3. The vehicle block calculates the actual vehicle speed and acceleration. The speed is a function of the traction, resistive and braking forces acting on the vehicle. The model is based on the balance of forces acting in the longitudinal direction.

In the supervisory off-line control problem, it is sufficient to study an abstracted scheme of the system. The power demand at the DC bus  $P_L$  is computed by taking the power train losses from the wheels until the input of the electric motor ( $P_{Losses}$ ). The losses include the transmission system losses and the motor/inverter losses. The driving cycle is usually a matrix indexed by time and speed ( $v$ ). The first step is to calculate the total forces ( $F_T$ ) acting on the wheel during each time step and then derive the power demand at the levels of the wheel ( $P_w$ ). The total sum of forces  $F_T$  acting on the wheels

are the aerodynamic force  $F_w$ , the force of rolling resistance or friction losses  $F_r$ , the force due to inclination or load slope  $F_i$  and the acceleration force  $F_a$ . These forces are described in equations (14)–(18). The power demanded by the vehicle as a function of speed at the level of the wheels is given in equation (19). For simplicity, the road is considered to be flat and therefore the road inclination ( $\theta$ ) is zero.

$$\text{Aerodynamic Force : } F_w = \frac{1}{2} \rho A_f C_w v^2 \quad (14)$$

$$\text{Rolling Resistance : } F_r = mg C_r \cos(\theta) \quad (15)$$

$$\text{Inclination Force : } F_i = mg \sin(\theta) \quad (16)$$

$$\text{Acceleration Force : } F_a = ma \quad (17)$$

$$\text{Sum of Forces : } F_T = F_w + F_r + F_i + F_a \quad (18)$$

$$\text{Power Demand at Wheels : } P_w = v F_T \quad (19)$$

The losses in the transmission system are derived from the efficiency map samples of the gearbox which is approximated at 95 percent. Similarly, the power losses of the electric motor and inverter system are calculated based on the motor efficiency map which is shown in Fig. 7. These losses are added to the load power at the level of wheels to derive the power demanded by the electric motor as shown in equation (20).

$$\text{Power Demand at Motor : } P_L = P_w + P_{Losses} \quad (20)$$

### The energy management system block

The main subsystem in the FCHV is the energy management system block. The EMS block is the main drive of the FCHV since it organizes the power allocation between the FC system and the battery system. The algorithm that is dealt with in this

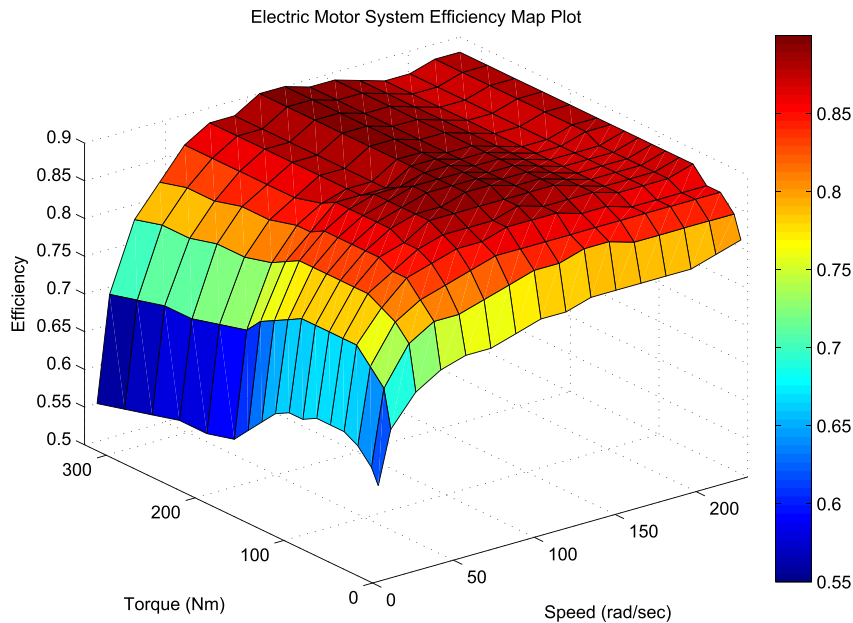


**Fig. 7 – Motor losses.**

paper exhibits a slow response time especially when compared to the vehicle's response time. For this reason, the EMS is tweaked for it to be adaptable to all algorithmic scenarios. This is accomplished by using lookup tables linked directly to the output of the algorithmic blocks in the Matlab files environment. Therefore, the off-line Matlab weighted DP program generates the matrix of optimum power allocation value which contains the power levels of the FC, battery and braking power ( $P_{br}$ ) at each step of time, along with the torque required by the electric motor ( $T_m$ ). Then this matrix is fed to the EMS of the Simulink model using look-up tables as shown in the topology of Fig. 8.

The FC status ( $S_{FC}$ ) block pinpoints the conditions in which the FC is turned on or off. There are four lookup tables embedded in the EMS block. These lookup tables are derived beforehand from the algorithmic techniques discussed in the forthcoming sections. All tables are horizontally indexed by the cycle time of the FCHV. Vertically, they are indexed by the FC power requirements, motor torque request and braking power request respectively. Fig. 8, reveals a topological view of the above mentioned design. The FCHV Simulink model is based on net current calculations and not power computations. For this reason the FC and battery power requests are translated into current request by dividing those requests with the corresponding voltage at the DC bus.

## Dynamically efficient energy management system

Mathematical optimization is a technique utilized to achieve the best possible outcome for a certain problem. It can take different forms depending on the type of the objective function. The numerical formulation of the FCHV power train exhibits nonlinear equations. Therefore, it is crucial to select an optimization technique that will closely model the drive train of the FCHV in-order to lead optimum results. The goal is to optimize the power allocation between the FCHV sources which are the FC system and the battery system. This optimization is performed off-line using Matlab software. After the optimal power allocation matrix is obtained, it is injected into the EMS of the Simulink model that is explained in the previous section.

### IDP general formulation

Improved dynamic programming is an upgraded version of DP through which the number of states at each level does not change with time. It bypasses the problem of dimensionality suffered using dynamic programming. In such a supervisory control model, an objective function along with the constraints is defined. The independent variables are defined

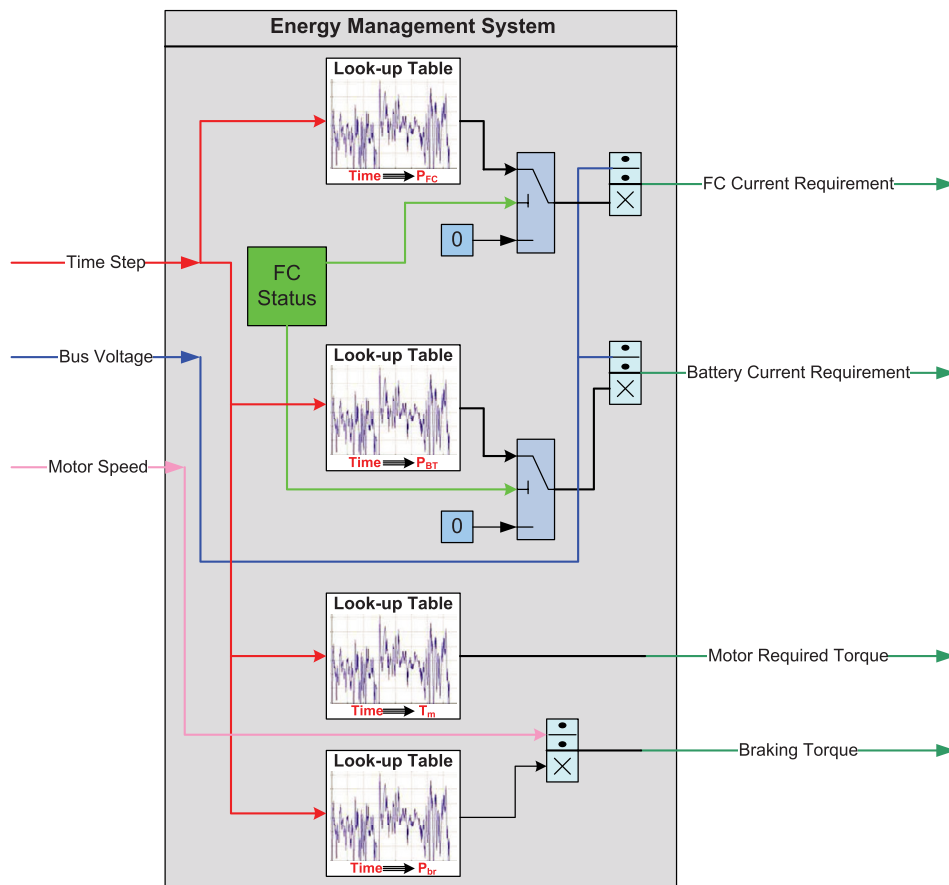


Fig. 8 – EMS topological model.

through a set of actions and the dependent variables are defined in a number states.

The time horizon is sampled into  $T$  discrete stages that are equally spaced along the length of the driving cycle. The vertical axis is quantized into  $S$  different states. The state vector  $u$  is composed of fuel cell power levels that range from 0 to  $P_{FCmax}$  in equal steps. The paper deals with the power allocation of the fuel cell and battery to minimize the cost function. For this reason, the power of the fuel cell or the power of the battery can be considered as the state vector. By fixing one, the other can be derived from the power balance equation, hence this power fixing method lends itself for an easier solution of the problem and is natural to program. In this case, the supervisory control of the vehicle is exerted by the fuel cell, and then the battery satisfies the remaining power demand within the SOC constraints. Fig. 9, reveals a model of the network along with all interconnected nodes.

The total number of nodes is  $S \times T$  which depends on the number of selected states and time samples. Each of these nodes ( $N$ ) is indexed according to its current stage location and corresponding state. For example node  $N_{iu_j}$  corresponds to the node at stage  $i$  and state  $u_j$ . At the first stage each node is characterized with a cost function  $C_{iu_j}$ , symbolized as nodal cost. This is a discrete closed form function that defines a certain objective. The nodal cost represents the cost of being in the associated state. Starting the second stage until  $t = T$ , each node has two associated costs which are the nodal cost and the transition cost. The transition cost  $R_{u_k, iu_j}$  is the cost of moving from the previous states  $u_k$  at  $i - 1$  to the current state  $u_j$  at  $i$ . The total cost  $F_{iu_j}$ , associated with each node at a certain stage is the sum of its nodal cost and the minimum value of all transition costs to the node from previous stage as shown in equation (21).

$$F_{iu_j} = C_{iu_j} + \min_k [R_{u_k, iu_j}] \quad i = 1 : T; j, k = 1 : S \quad (21)$$

If a transition to a node or a certain state of the current node violates any of the constraints, then the node is infeasible and could not be considered in the optimum path. To remove it from the optimal path, a very high cost is associated with the transitional cost. The idea behind correlating a high cost rather than removing the transition node from the path is to ensure a faster algorithmic convergence in Matlab without adding extra functionalities. It is assumed that there is at least

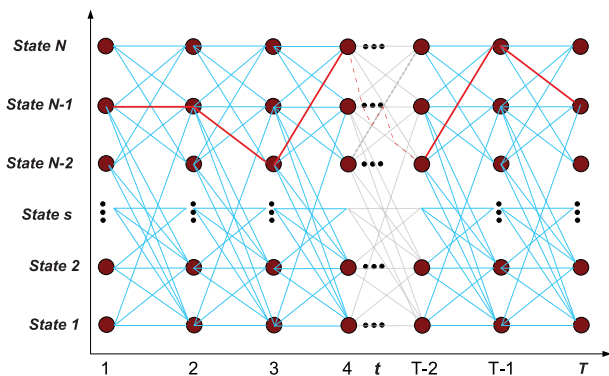


Fig. 9 – Improved dynamic programming sketch.

one possible transition  $g_{u_k, iu_j}$  that is feasible so removing a link from the path is meaningless. Finally, at stage  $T$ , the minimum cost  $F_{Tu_j}$  is selected and traced back to the first stage following the minimum cost path. The algorithm is depicted in steps in Algorithm 1. All index correlations are summarized in equation (22).

$$\text{Index : } \begin{cases} \text{State Vector : } u = [u_1 \ u_2 \dots u_j \dots u_S] & j = 1 : S \\ \text{Stage Vector : } Stage = [1 \ 2 \dots i \dots T] & i = 1 : T \\ \text{Node Representation : } N_{iu_j} \\ \text{Node Cost : } C_{iu_j} \\ \text{Transition Cost : } R_{u_k, iu_j} & k = 1 : S \end{cases} \quad (22)$$

**Algorithm 1** Improved DP Algorithm

- 1: {Forward Path Generation}
- 2: for  $i$  such that  $i = 1 : T$  do
- 3:   for  $j$  such that  $j = 1 : S$  do
- 4:     for  $k$  such that  $k = 1 : S$  do
- 5:       Compute  $C_{iu_j}$
- 6:       Compute  $R_{u_k, iu_j} \forall k$
- 7:       Locate minimum of  $R_{u_k, iu_j}$
- 8:       Save index of min  $Min = [i, k_{min}]$  for min of  $R_{u_k, iu_j}$
- 9:       Compute  $F_{iu_j} = C_{iu_j} + R_{u_k, iu_j} + C_{(i-1)u_k}$
- 10:     end for
- 11:   end for
- 12: end for
- 13: {Backward Path Trace}
- 14: for  $m$  such that  $m = 1 : T$  do
- 15:   Locate  $N^*(T) = \min(F_{Tu_j}) \forall j$
- 16:   Locate all  $N^* = \text{Min}(:, 2)$
- 17: end for

**Weighted non-linear IDP formulation for FCHV EMS**

The improved dynamic programming is formulated for the FCHV EMS. In this context, the nodal cost and the transitional costs are defined. The nodal cost shown in equation (23), calculates the cost of energy from the FC and battery. It also considers the braking energy as equivalent to the FC energy. This is due to the fact that this dissipated energy originally came from the FC. The cost of the FC includes the hydrogen consumption cost as well as a penalty factor. The latter is a fraction of the life of the fuel cell. In this manner, the cost function considers the life cycle of the FC. The cost of the battery is considered during charging and discharging phases. This cost comprises the depletion of the battery towards its end life.

$$C = \left[ \sum_{t=1}^T [(\gamma_{FC} + \gamma_{SL-FC})P_{FC}(t) + \gamma_{BT}P_{BT}(t)] \Delta t \right] \quad (23)$$

At each time step, the battery SOC needs to be updated according to equation (24). It is important to note that when the battery power is positive, the battery is considered to be discharging power and thus feeding the load. During this period the power supplied to the load by the battery is lower than the actual energy produced by the battery due to losses.

This is accounted for in equation (24) by splitting the operation of the battery into charging and discharging modes. When the power supplied by the battery is negative, the battery is considered to be charging and thus the load is generative. However, during this period the actual energy delivered to the battery is lower than that generated from the wheel's kinetic energy and so the efficiency is multiplied by the battery energy.

$$SOC_{iuj} = \begin{cases} SOC_{(i-1)uj} - \frac{P_{BT,iuj} \Delta t}{\eta_{BT} C_{BT}} & \text{if } P_{BT,iuj} \geq 0 \\ SOC_{(i-1)uj} - \frac{\eta_{BT} P_{BT,iuj} \Delta t}{C_{BT}} & \text{if } P_{BT,iuj} < 0 \end{cases} \quad (24)$$

In each state at a certain discrete time, it is important to adhere to the power equation represented in equation (25):

$$P_{FC,iuj} + P_{BT,iuj} - P_{br,iuj} = P_{Li} \quad (25)$$

Transitional costs are linked to the feasibility of a step from a node to the other. If the jump from a node to the next is infeasible then a very high cost is associated with the transitional cost. On the contrary, if a link is feasible between the nodes then a zero cost defines the transitional cost. This feasibility of a move is verified through the fact that the power source variables adhere to their limits as defined by equations (26)–(30). If a step violates the above limits then it will be an infeasible state. The limits are the FC lower ( $P_{FCmin}$ ) and upper ( $P_{FCmax}$ ) power limits, the battery lower ( $P_{BTmin}$ ) and upper ( $P_{BTmax}$ ) power limits, the SOC lower ( $SOC_{min}$ ) and upper ( $SOC_{max}$ ) limits, the FC ramp rates lower ( $R_{down-FC}$ ) and upper ( $R_{up-FC}$ ) limits and the battery ramp rates lower ( $R_{down-BT}$ ) and upper ( $R_{up-BT}$ ) limits.

$$\text{Fuel Cell Power Limits : } P_{FCmin}(t) \leq P_{FC}(t) \leq P_{FCmax}(t) \quad (26)$$

$$\text{Battery Power Limits : } P_{BTmin}(t) \leq P_{BT}(t) \leq P_{BTmax}(t) \quad (27)$$

$$\text{Battery SOC Limits : } SOC_{min}(t) \leq SOC(t) \leq SOC_{max}(t) \quad (28)$$

$$\text{FC Ramp Rate : } R_{down-FC} \Delta t \leq P_{FC}(t) - P_{FC}(t-1) \leq R_{up-FC} \Delta t \quad (29)$$

$$\text{BT Ramp Rate : } R_{down-BT} \Delta t \leq P_{BT}(t) - P_{BT}(t-1) \leq R_{up-BT} \Delta t \quad (30)$$

After the forward algorithm terminates, then the node at  $t = T$  that corresponds to the minimum cost among the set of nodes at the final stage is chosen. Afterwards a backward algorithm traces the optimum nodes corresponding to that node all the way towards the beginning. This backward traced path represents the optimal path.

The formulation of the non-linear IDP for electric vehicles consists of a fitness function ( $V$ ) that consists of several factors in an attempt to achieve the desired response of the system as shown in equation (31).

$$V_{iuj} = w_a P_{FC,iuj}^2 \Delta t + w_b P_{BT,iuj}^2 \Delta t + w_c [SOC_{br,iuj} - SOC_r]^2 \Delta t \quad (31)$$

The first component considers the power consumption from the fuel cell which should be limited in-order to guarantee minimum hydrogen consumption. The hydrogen consumption cost equation used is shown in equation (3). The second factor ensures the battery power limits in-order not to

over-use the battery in terms of frequent charging and discharging. The third factor is responsible to provide a healthy tunnel for the battery SOC so as to keep it around a certain value. For optimum operation of the FCHV, it is of keen importance for the SOC not to drop below 20% to preserve the life of the battery. Moreover, it is desirable for the SOC not to rise above 80% in-order to capture energy from regenerative braking. The battery non-linear charge and discharge efficiencies are considered from equation (13). The weights ( $w_a$ ,  $w_b$ ,  $w_c$ ) are updated in-order to find the minimum cost for a certain set of weights.

This weighting method is necessary, especially for large driving cycles. The IDP method is limited to the number of states at each level and does not consider all possible combinations like the normal dynamic program does. For this reason, the system can go into unfeasible states and thus fail to converge at a higher samples of time. For this reason, weights are added that are specific for each cycle to guarantee convergence. The calculations of the weight for the highway and FUDS driving cycles are explained in the next section. If the driving cycle is small or limited then the weights are removed and the fitness function is substituted with the normal non-linear cost function in equation (23). This guarantees faster convergence.

### Weight analysis

In this section, the value of the weights of the IDP objective function is calculated using a customized brute-force search algorithm that yields the minimum cost and favorable SOC limits. Brute-force search algorithm is a problem solving technique based on itemizing all possible candidates of the solution and then choosing the best fit candidate that abides by the problem objective function. At each step the program has to evaluate the effect of weight change by running the IDP algorithm which is time consuming. For this reason not all possible candidates will be evaluated and thus a customized brute-force search algorithm with weights ranging from 1 till 100,000 in multiples of 10 is chosen. The main algorithm needs  $O(n^5)$  and each IDP run takes  $O(m^2)$  which makes the overall runtime close to  $O(n^5) \times O(m^2)$ . During the weight calculations, three variables are involved which correspond to the weights while in the IDP algorithm, approximately six variables are computed.

The optimum value of the weights depends on the demanded power. The main trade-off to reach a steady state optimal value of the weights is between the total cost and the desirable range of SOC during the trip. For this reason, the program is set to locate the optimum weights that can achieve a minimum cost and an SOC profile that maintains 0.2 as its lowest limit. The two binding variables are the power from the FC and the battery. These two variables play an important role in maintaining the balance between the system cost and the SOC profile. The optimal weights for the corresponding driving cycles is indicated in Table 4. It is noticed from the table that for urban cycles that battery power weight is equal to the FC power weight while for the highway cycle it is less. This is verified by the fact that urban cycles tend to exploit the battery more by the frequent charging and discharging and for this reason higher weight will preserve the battery life.

**Table 4 – Driving cycle optimum weights.**

	wa	wb	wc
Highway	1000	100	1
FUDES	1000	1000	1

### State machine control algorithm for comparison methodology

The proposed methodology is compared against a state machine control algorithm. The latter is proposed and tested by Panik [26]. Different states are formulated depending on the demanded power and the battery SOC. It is composed of seven states. First, if the demanded load is positive and greater than the minimum power that can be supplied by the FC, then the FC system is turned on and limited to the minimum power value. The battery system supplies the difference between the required load and minimum power value of the FC. Second, when the demanded load is positive and ranges between the minimum and maximum power that can be supplied by the FC, then the FC system is turned on and limited to the demanded power values while preserving the ramp rate constraint. The battery system supplies the difference between the required load and supplied power value of the FC. Third, if the demanded load is positive and is greater than the maximum power that can be supplied by the FC, then the FC system is turned on and limited to its maximum power value while preserving the ramp rate constraint. The battery system supplies the difference between the required load and supplied power value of the FC. Fourth, if the demanded load is generative and is greater than the minimum power that can be endured by the motor, then the FC system is turned on and limited to its minimum power value. The battery system supplies the difference between the required load and supplied power value of the FC. Fifth, if the demanded load is generative and is less than the minimum power that can be endured by the motor, then the FC system is turned on and limited to its minimum power value. The battery system supplies the difference between the minimum motor power and the supplied power value of the FC. Sixth, if the demanded load is in idle mode and is less than the minimum power that can be supplied by the FC system, then the FC system is turned on and limited to its minimum power value. The battery system supplies the difference between the auxiliary power demand and the supplied power value of the FC. Finally, if the demanded load is in idle mode and is greater than the minimum power that can be supplied by the FC system, then the FC system is turned on and limited to its minimum power value while preserving the ramp rate constraint. The battery system supplies the difference between the auxiliary power demand and the supplied power value of the FC.

### Testing for known driving cycle

The weighted IDP is applied, tested and analyzed for known driving cycles. A multiple of simulated comparative experiments demonstrates the efficiency, significance and

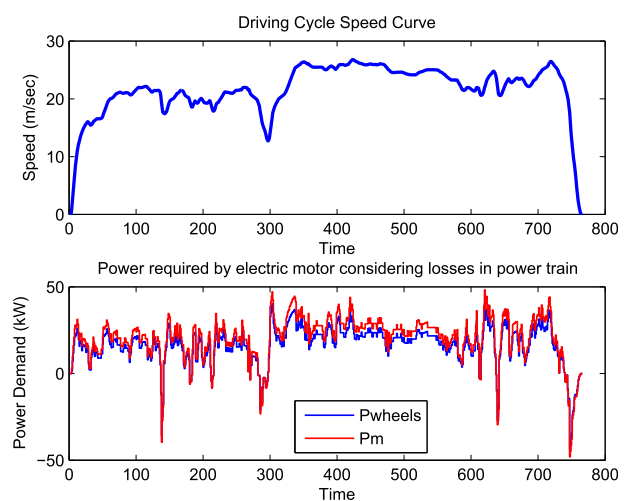
applicability of the algorithmic strategy. The outcome of the algorithm is the optimal power split between the FC and the battery. This is injected in the vehicle Simulink model which incorporates also a PID controller. The behavior of the system resources and electric motor is analyzed and the hydrogen consumption is compared against the state machine controlled algorithm.

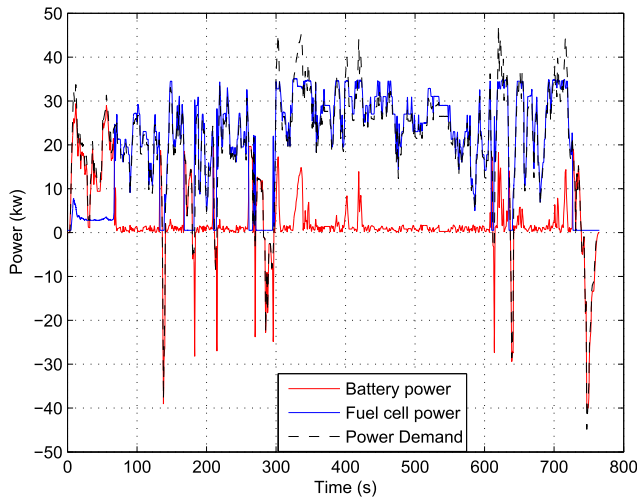
The power profile of the highway driving cycle is shown in Fig. 10. The upper curve indicates the speed profile over the 766 ss period. The lower curve shows the calculated demand at the wheels and the electric motor after the losses are added.

The power allocation profile of the light duty sprinter operating on a highway driving cycle as derived from the Simulink model is shown in Fig. 11.

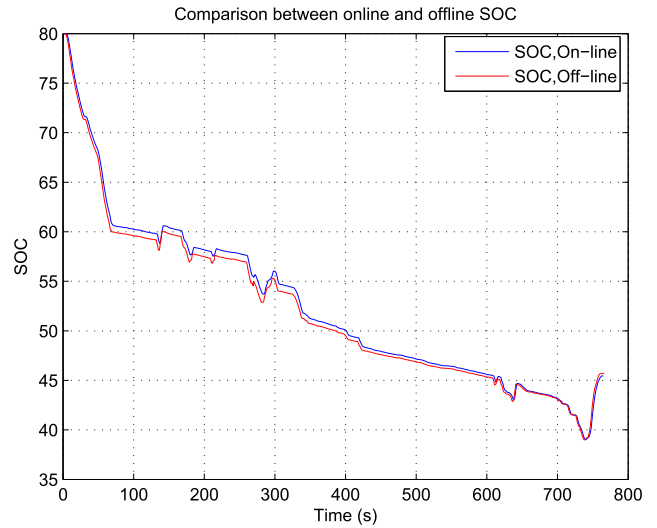
The FC is supplying the demanded load almost throughout the cycle. This coincides with the fact that the sprinter has a small battery and a large FC which makes the later the main energy source in the system. To relieve the stresses on the FC, the battery tends to aid the FC in supplying the load at several instances of time. At 320,400,420 and 620 s the battery supplied the load with power aided by the FC. During these times the demand is high, so by aiding the FC, the battery helped to relieve the stresses of the FC. This is the result after the simulation of the optimal power allocation matrix in Simulink environment. The sources ramp rates are respected during this time as shown in Fig. 12. At a certain instance the fuel cell exceeded its ramp rate limit, the minimum limit is set to 10 kW/s and a maximum limit of 20 kW/s is allowed. However, the paths where the minimum limit is exceeded are penalized. On the other hand, the paths where the maximum limit is exceeded, are considered infeasible. The FC continues to supply the load aided by the battery at certain instances of time. It is noticed that the FC power is higher than the load, to cater for the power needed for FC compressor and auxiliaries. When the load is generative, the battery charges power through regenerative braking.

Fig. 13 shows the SOC profile of the cycle. The software is trying to keep the SOC within the favorable limits and thus SOC is not dropping below 20%. The figure shows the

**Fig. 10 – Highway power profile.**



**Fig. 11 – Highway cycle-sprinter power allocation of the sources.**



**Fig. 13 – Highway cycle-sprinter battery SOC profile.**

approximate match between the battery SOC during on-line and off-line optimization.

Fig. 14, indicated the approximate match between the on-line and off-line results in terms of FC power and battery power of the simulation.

The speed profile of the FUDS driving cycle as indicated by the Simulink model is shown in Fig. 15. The cycle is characterized by low speeds and fast dynamics especially because the cycle shifts between accelerating, decelerating and idling states. This will induce negative and positive fluctuations in the power profile.

In Fig. 16, the simulation shown is between 0 till 450 s. The battery is charging every time the load is generative. It is aiding the battery in supplying the load so as to lower the hydrogen consumption especially when high loads are

encountered such as at 200 s. The battery plays a more active role in this cycle as compared to highway cycle due to its frequent charging. The power allocation profile of the light duty sprinter operating on FUDS driving cycle shows that the battery is being charged and discharged often due to the fact that urban cycles are rich in generative loads due to the frequent idling mode. Fig. 17 shows the SOC profile of the cycle match between the SOC during off-line and on-line simulation.

Table 5, shows the results which include costs and hydrogen consumption levels. ECMS percentage reflects the percentage of energy that is used to charge the battery from the fuel cell rather than regenerative braking. The desirable value of this variable is zero so as not to waste hydrogen supply. The program succeeded in keeping the ECMS

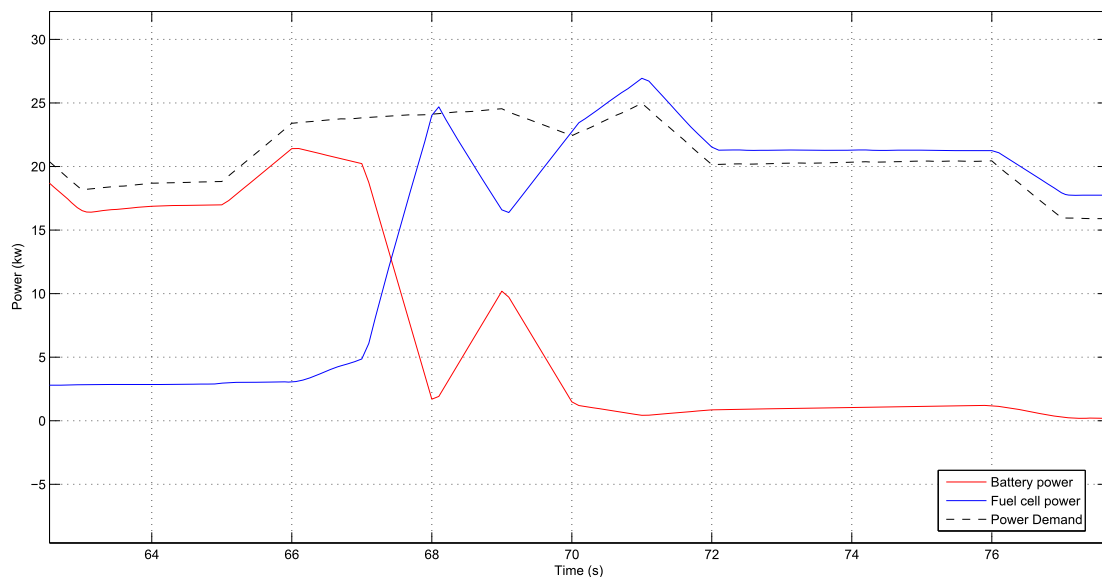


**Fig. 12 – Episode 1 – ramp rates – power allocation of the sources.**

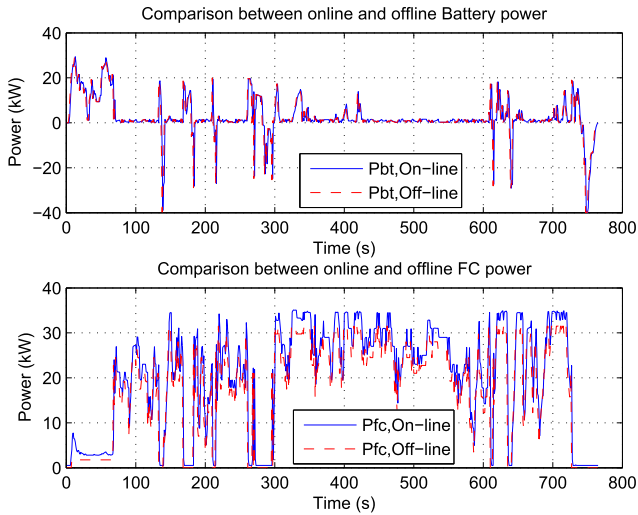


Fig. 14 – Highway cycle-on-line, off-line source comparison.

percentage as low as possible so as not to charge the battery using hydrogen energy. In FUDS cycle, ECMS percentage is kept at zero level because the battery is already charging from the regenerative braking due to the cycles fast dynamics.

Haar wavelet transform is the simplest transform that can divide a signal into its low and high frequency components. Its main disadvantage is that it is not continuous and thus not differentiable, however it exhibits advantageous results with signals incorporating sudden transitions. It was used for stress analysis on FCHV sources by the authors in Ref. [6]. The power supplied by the FC and the battery for a given load is decomposed using Haar wavelet transform. The decomposition results in a low and a high frequency component of the signal. It is noticed that the high frequency component has a zero mean and so the standard deviation is used as a measure to indicate the stress component on the source. The stresses on the system components is higher for the FC than the battery for the highway cycle. The latter means that the sudden

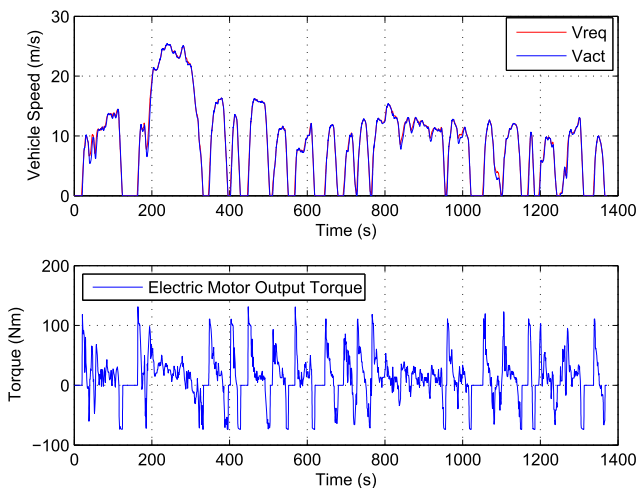


Fig. 15 – FUDS power profile.

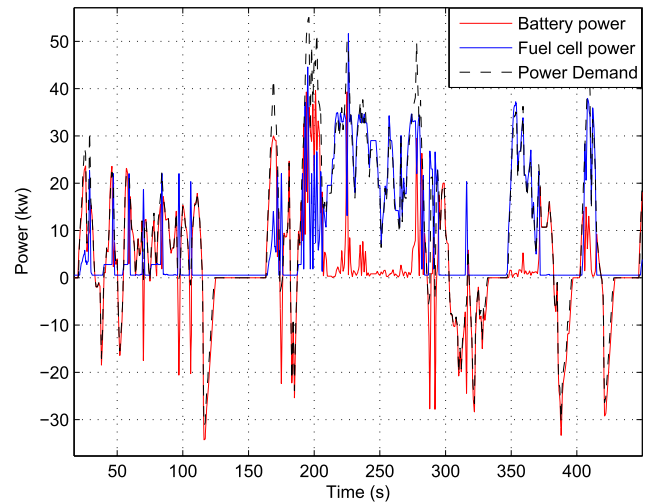


Fig. 16 – Episode 1 – FUDS cycle-sprinter power allocation of the sources.

changes in power levels of the system sources is more on the FC side and thus the FC is exploited more. This is normal for highway cycles because the fast dynamics don't provide a room for battery to charge and discharge frequently. Such sudden changes add stresses to the components. For instance if the FC is supplying 5 kW now, it is better to maintain this supply rather than shifting between 5 and 0 kWS or 5 and 20 kW. The stresses on the FC and battery systems are 11.4 and 12.7 respectively for the FUDS cycle. This indicates that in fast dynamics driving cycles more stresses occur to the battery. It is justified by the frequent idle state visited during urban cycles which increases regenerative braking via kinetic energy recuperation and thus drains the battery more.

The overall efficiency is a measure of meeting the load demand at each instance of time. The higher this value is the more the demand is met. Equation (32) shows the mathematics behind such a measure of performance. The latter is

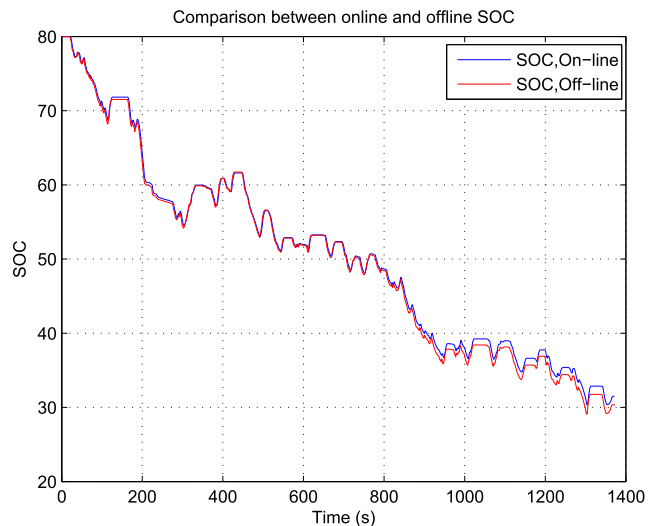


Fig. 17 – FUDS cycle-sprinter battery SOC profile.

**Table 5 – Highway/FUDS driving cycle results.**

Variable	Highway	FUDS
The cost of operation (\$)	2.76	1
Percentage FC cost (%)	1.4	1.5
Percentage BT cost (%)	0.54	0.7
Percentage H <sub>2</sub> cost (%)	98	97.7
H <sub>2</sub> fuel consumption (g)	179	65.2
H <sub>2</sub> fuel consumption (g/km)	10.89	5.9
ECMS percentage	0.7059	0
Fuel cell stress factor	15.9	11.4
Battery stress factor	11.03	12.7
Overall efficiency	99.77	100
Runtime (second)	10	14

approximated at around 99.77% which means that the demand was met 99.77 percent of the time for the highway cycle and 100% for the FUDS cycle.

$$\eta = \frac{P_L}{P_{FC} + P_{BT}} \quad (32)$$

Table 6 dictates the comparison of this methodology for highway cycle against the state machine control algorithm. Concerning cost and hydrogen consumption levels, it is noticed that those are the highest using the RB method. The latter does not foresee the power profile and thus performs a per step optimization which blinds it from locating the optimal allocation range. However, since it does not require any optimization steps, it has the fastest runtime. The savings in hydrogen consumption when non-linear IDP is incorporated is around 15% as compared to RB. As for the FUDS cycle against the state machine control algorithm, the first eye-catching result is the high consumption rate of the RB method due to lack of foreseeing the cycles, however they have the fastest runtime. Savings in hydrogen consumption of up to 50% is achieved using nonlinear IDP.

## Conclusions

This paper aims to present a methodology to optimize the controller of an FCHV based on a weighted improved dynamic programming technique and PID controller. The problem formulation takes into account the life-cycle cost of the system components and considers minimizing hydrogen usage along with operational cost. Detailed Simulink model of the vehicle subsystems is built. Test simulations were performed on known driving cycles. The objective is to develop a conceptual approach for an energy optimization approach which

**Table 6 – Highway/FUDS driving cycle comparative results.**

	Highway		FUDS	
	IDP	RB	IDP	RB
Operational cost (\$)	2.7	3.2	1	2.2
H <sub>2</sub> consumption (g)	179	211	65.2	143
Runtime (s)	10	3	14	3

is able to consider a wide range of constraints and targets. The simulations in this paper serve to explain and to prove the process. Comparison against a state control based EMS indicates that the system cost can be reduced depending on the driving cycle. The weighted non-linear IDP is formulated considering the non-linear hydrogen consumption curve of the FC and the non-linear battery Q-maps. Weights are used to achieve a definite and faster convergence. They are approximated using a brute force method. The performance criteria is based on the overall operational cost as well as the hydrogen consumption per trip. Moreover, battery state of charge and system efficiencies were also measured and analyzed. The stresses on the FCHV subsystem sources are approximated based on a wavelet transform of instantaneous power of the system sources. More stresses are added on the battery in urban cycles than on highway cycles. The technique succeeded in keeping ECMS percentage low so as not to exploit hydrogen levels by charging the battery. The overall efficiency ensured that the load demand is met at each instance of time. Comparison between off-line and on-line simulations shows a great match between the power curves of the sources and the battery SOC curve. Our technique was superior over the state machine control algorithm with respect to hydrogen consumption savings which was around 15% for highway cycles. As for the FUDS cycle savings in the hydrogen consumption of up to 50% is achieved using the weighted nonlinear IDP. Future work will apply this technique in smaller chunks to target real time optimization.

## Acknowledgments

The authors would like to acknowledge the support provided both by the American University of Beirut and the University of Applied Sciences for conducting this research. Moreover, special thanks to Mr. Ying Huang for helping us build the Simulink model of the FCHV.

## REFERENCES

- [1] Zheng Y, Dong ZY, Xu Y, Meng K, Zhao JH, Qiu J. Electric vehicle battery charging/swap stations in distribution systems: comparison study and optimal planning. *IEEE Trans Power Syst* 2014;29:221–9.
- [2] Vural B, Dusmez S, Uzunoglu M, Ugur E, Akin B. Fuel consumption comparison of different battery/ultracapacitor hybridization topologies for fuel-cell vehicles on a test bench. *IEEE J Emerg Sel Top Power Electron* 2014;2:552–61.
- [3] Torreglosa J, Garcia P, Fernandez L, Jurado F. Predictive control for the energy management of a fuel-cell battery supercapacitor tramway. *IEEE Trans Indust Inform* 2014;10:276–85.
- [4] Bayindir KC, Gozukucuk MA, Teke A. A comprehensive overview of hybrid electric vehicle: powertrain configurations, powertrain control techniques and electronic control units. *Energy Convers Manag* 2011;52:1305–13.
- [5] Erdinc O, Uzunoglu M. Recent trends in {PEM} fuel cell-powered hybrid systems: investigation of application areas, design architectures and energy management approaches. *Renew Sustain Energy Rev* 2010;14:2874–84.

- [6] Motapon S, Dessaint LA, Al-Haddad K. A comparative study of energy management schemes for a fuel-cell hybrid emergency power system of more-electric aircraft. *IEEE Trans Indust Electron* 2014;61:1320–34.
- [7] Brahma A, Guezennec Y, Rizzoni G. Optimal energy management in series hybrid electric vehicles. In: *Proceedings of the 2000 American Control Conference*, vol. 1; 2000. p. 60–4.
- [8] Wood AJ, Wollenberg BF. *Power generation operation and control*. 2nd ed. New York: Wiley; 1996.
- [9] Bellman R. *Dynamic programming*. 1st ed. Princeton; 1957.
- [10] Rurgladdapan J, Uthaichana K, Kaewkham-ai B. Li-ion battery sizing and dynamic programming for optimal power-split control in a hybrid electric vehicle. In: *9th International conference on electrical engineering/electronics, computer, telecommunications and information technology*; 2012. p. 1–5.
- [11] Vinot E, Trigui R, Cheng Y, Bouscayrol A, Espanet C. Optimal management and comparison of SP-HEV vehicles using the dynamic programming method. In: *Vehicle power and propulsion conference (VPPC)*; 2012. p. 944–9.
- [12] Xu L, Ouyang M, Li J, Yang F. Dynamic programming algorithm for minimizing operating cost of a PEM fuel cell vehicle. In: *IEEE international symposium on industrial electronics (ISIE)*; 2012. p. 1490–5.
- [13] Dokuyucu H, Cakmakci M. Concurrent design of energy management and vehicle stability algorithms for a parallel hybrid vehicle using dynamic programming. In: *American control conference (ACC)*; 2012. p. 535–40.
- [14] Prez LV, Bossio GR, Moitre D, Garca GO. Optimization of power management in an hybrid electric vehicle using dynamic programming. *Math Comput Simul* 2006;73:244–54.
- [15] Shen C, Chaoying X. Optimal power split in a hybrid electric vehicle using improved dynamic programming. In: *Power and energy engineering conference (APPEEC)*; 2010. p. 1–4.
- [16] Ning Q, Xuan D, Kim Y. Modeling and control strategy development for fuel cell electric vehicles. *Int J Automot Technol* 2010;11:229–38.
- [17] Ryu J, Park Y, Sunwoo M. Electric powertrain modeling of a fuel cell hybrid electric vehicle and development of a power distribution algorithm based on driving mode recognition. *J Power Sources* 2010;195:5735–48.
- [18] Dalvi A, Guay M. Control and real-time optimization of an automotive hybrid fuel cell power system. *Control Eng Pract* 2009;17:924–38.
- [19] Ansarey M, Panahi MS, Ziarati H, Mahjoob M. Optimal energy management in a dual-storage fuel-cell hybrid vehicle using multi-dimensional dynamic programming. *J Power Sources* 2014;250:359–71.
- [20] Suh K-W, Stefanopoulou A. Coordination of converter and fuel cell controllers. In: *Proceedings of the 2005 IEEE international symposium on intelligent control*; 2005. p. 563–8.
- [21] Spindelov J, Marcinkoski J. *Fuel cell system cost*. DOE Fuel Cell Technologies Office; 2013.
- [22] *Hydrogen Economy*. Wikipedia the free encyclopedia. 2013.
- [23] *Battery and Energy Technologies*. Electropaedia. 2014. [www.mpoweruk.com](http://www.mpoweruk.com).
- [24] *Annual energy outlook*. 2012. DOE/EIA-0383, [www.eia.gov](http://www.eia.gov).
- [25] Bernard J, Delprat S, Guerra T, Bchi F. Fuel efficient power management strategy for fuel cell hybrid powertrains. *Control Eng Pract* 2010;18:408–17.
- [26] Panik F. Simulation studies concerning a fuel cell hybrid bus. 2009. SAE Technical Paper 2009-36-0402.